



Mechanically tuning magnetism and transport property in spin gapless semiconductor CoFeMnSi flexible thin film

Fangqing Xin ^a, Caiyin You ^{a,*}, Huarui Fu ^a, Li Ma ^a, Zhenxiang Cheng ^b, Na Tian ^a

^a School of Materials Science and Engineering, Xi'an University of Technology, Xi'an, 710048, PR China

^b Institute for Superconducting & Electronic Materials, University of Wollongong, NSW, 2500, Australia

ARTICLE INFO

Article history:

Received 27 June 2019

Received in revised form

5 September 2019

Accepted 7 September 2019

Available online 9 September 2019

Keywords:

Spin gapless semiconductor
Semiconductor-metal transition
Bending tunability
Magnetism

ABSTRACT

The potential spin gapless semiconductor CoFeMnSi is one of most promising materials used in the potential spintronics devices. In this work, we realized the semiconductor-like behavior of CoFeMnSi thin film deposited on the fluorophlogopite substrate, and achieved a flexible CoFeMnSi film by exfoliating the substrate. The film grown on the fluorophlogopite substrate exhibits a partial $L2_1$ ordered structure after annealing at 300 °C. The bending tunability of the transport and magnetic properties were investigated. The semiconductor-metallic like transition can be varied through bending. The in-plane coercivity could be tuned up to 440% under a bending curvature of 1.9 mm. Interestingly, an exchange bias was observed in CoFeMnSi thin film. XPS analyses show that there exists the bonding of oxides at the interface between CoFeMnSi layer and substrate. Thus, it could be deduced that the antiferromagnetic coupling occurs along the interface, causing an exchange bias.

© 2019 Elsevier B.V. All rights reserved.

1. Introduction

Recently, the flexible electronics devices are widely pursued for the potential applications as the flexible displays, flexible sensors and smart wearable devices [1,2]. Among them, the magnetic materials with high spin polarization as well as excellent mechanical flexibility are highly desirable in the flexible spintronics devices. The prerequisite of realizing the potential application of flexible spintronics devices is of understanding the tunability of the flexible magnetic films. The fluorophlogopite (F-mica) was considered to be suitable as the flexible substrate because the F-mica is connected layer-by-layer through van der Waals forces and easy to be mechanical exfoliated [3] other than the merits of the flat surface and high-temperature-tolerance character [1,4]. The relevant studies of tunable magnetism have been reported in the systems of F-mica/Fe₃O₄ [5], F-mica/CoFe₂O₄ [6,7] and F-mica/CuFe₂O₄ [8]. It was also found that the stable magnetism was realized in the stacks of F-mica/(Pt/Co)/Ru/(Co/Pt)₂ [9] and F-mica/LiFe₅O₆ nanopillar array [10]. However, there are very few investigations about the flexible magnetic films of the potential high spin polarized materials.

On the other hand, the potential spin gapless semiconductors

(SGSs) were attracting more attentions since it was introduced by Wang in 2008 [11]. These materials are very sensitive to the external pressure due to their particular band structure that one spin channel exhibits a zero-band gap and another spin channel shows semiconducting band gap [12–16]. Due to the unique band structures, they have been predicted to have some attractive properties including 100% spin polarization in theory, high carrier mobility and high resistance [11,14,15]. Some Heusler alloys including half-Heusler alloys, full-Heusler alloys, DO₃-Heusler alloys and LiMgPbSn-type quaternary alloys have been predicted to be SGSs [17]. Among these material candidates, the quaternary LiMgPbSn-type Heusler alloys CoFeMnSi, CoFeCrAl, CoMnCrSi, CoFeVSi and FeMnCrSb have been proved to be SGSs by theory [14]. Recent works have been reported that a Curie temperature and saturation magnetization value of CoFeCrAl thin film are about 390 K and 2 μ_B/f.u., respectively [18]. The saturation magnetization value of CoFeCrAl bulk is higher than thin film [19]. The high resistivity and its temperature dependence provide the evidence of SGS feature for CoFeCrAl alloy [19,20].

CoFeMnSi (CFMS) has been proved to be a spin gapless semiconductor (SGS) by experimental evidence, and CFMS bulk has a saturation magnetization of 3.7 μ_B/f.u. and Curie temperature of ~620 K, which is much higher than that of CoFeCrAl [13]. There are already some works performed on CFMS thin film including intrinsic properties [13,16,21,22], electric-field tuning of magnetism

* Corresponding author.

E-mail addresses: caiyinyou@xaut.edu.cn, caiyinyou@yahoo.com (C. You).

[12] and realization of PMA [23] on the rigid substrates like MgO and PMN-PT. But the fabrication of flexible CFMS thin film was not reported and its bending tunability of magnetism is an empty issue. In this work, we successfully realized flexible CFMS thin films and studied their bending tunability of transport and magnetic properties.

2. Experimental

Three sets of samples were fabricated: CFMS (10 nm), CFMS (20 nm), and CFMS (10 nm)/Pd (2 nm) (hereinafter refer to CFMS (10 nm)/Pd). The Heusler CFMS thin films were all deposited on F-mica substrates by magnetron sputtering at room temperature. The base pressure of sputtering chamber is better than 5×10^{-5} Pa. The purity of CFMS target was better than 99.9%. The CFMS layer was deposited under Ar pressure of 1 Pa with the DC power of 40 W. The electrode of Pd layer was deposited under Ar pressure of 0.5 Pa with the DC power of 25 W. The films were all annealed at a temperature of 300 °C for 30 min under a vacuum below 10^{-4} Pa.

The surface topography of the film was determined by an atomic force microscopy (Dimension Icon). The microstructure of the film was examined by transmission electron microscopy (TEM: JEM-2100F). The electric transport property measurement system (East Changing Technologies, China, ET9000) was used to detect the resistivity as the function of temperature ranging from 80 K to 300 K. The electronic structure of CoFeMnSi was calculated by using CASTEP based on density functional theory (DFT) within generalized gradient approximation (GGA). In our case, the plane-wave basis set cutoff is set as 340 eV. The $14 \times 14 \times 14$ mesh of special k-points was involved in the Brillouin zone for all calculations. The structure of CoFeMnSi is firstly optimized to reach a minimal free energy. The SCF convergence criterion for the calculation was selected as a difference of 5×10^{-6} eV/atom. The dependence of Hall resistivity on the magnetic field and magnetic property were characterized at 300 K by physical property measurement system (PPMS, QUANTUM DESIGN DYNACOOOL 9T) under the different curvatures. The different curvatures were realized by using the different glass convex holder with various curvature radius of 1.6, 2.5, and 7.5 mm respectively, in which the films were pasted. The elemental chemical states at the interface of the CoFeMnSi thin film with F-mica substrate were characterized by XPS (ESCALAB 250Xi).

3. Results and discussion

Film microstructure, surface morphology and flexibility were tested as shown in Fig. 1. Fig. 1(a) gives the bright field TEM image of CFMS (10 nm) grown on the F-mica substrate. Nanoscale polycrystalline structure is achieved. The inset of the selected area diffraction pattern presents the ordered diffraction rings of $B2$ (222) and $L2_1$ (311), indicating an ordered structure. A weak CoO diffraction ring appears which could be originated from the interfacial reaction along the interface with the oxide substrate. Fig. 1(b) is the high resolution TEM image (HRTEM), exhibiting the feature of nanograins around 10 nm or so surrounded by amorphous regions. The surface topography of the annealed film at 300 °C was shown through AFM image over $5 \times 5 \mu\text{m}$ area in 2-dimensional space in Fig. 1(c). The average roughness (R_a) of the thin film is about 0.998 nm. Since the F-mica substrate is a layered structure, which can be mechanically exfoliated layer by layer. While the substrate was exfoliated to be about 35 μm , the film becomes very flexible as shown in Fig. 1(d). It can be bent with a radius of curvature (ROC) of 1.9 mm without any crack.

As shown above, the partially ordered structure was achieved for the annealed film, implying the potential spin gapless semiconductor behavior [14,17]. Fig. 2(a) and (b) give the dependence of

the resistivity on the temperature from 80 K to 300 K for the films at the even state and bending status with ROC of 7.5 mm. Within the range of the measuring temperature, the resistivity of the flat film exhibits a semiconducting-like behavior. But under the bending state, the resistivity of film presents a transition from the semiconducting to metallic tendency around a temperature of 225 K with increasing the measuring temperature. To clarify this transition of conduction behavior after bending, we calculate the majority-spin band gap based on density functional theory for CFMS w/o bend. Here we obtain the bending effect through changing the lattice constants of CFMS (hereinafter referred to the bent CFMS). Fig. 2(c) shows the calculated majority-spin band structures of ordinary and bended CFMS. As shown in the inset of Fig. 2(b), the major strain appears along the bending direction of film plane and the strain along the other directions (perpendicular to bending direction in the film plane and film thickness direction) should be very trivial. So as to reach the real status more or less, we defined the bent CFMS with an expanded lattice constant a of 1% and constant lattice parameters $b = c = 5.65 \text{ \AA}$. It is clear that the majority spin presents a small band gap of $E_g = 0.021 \text{ eV}$ between the bottom of conduction band and the top of the valence band as seen in Fig. 2(c) marked with blue line. Under 1% strain, the band gap of majority spin was narrowed to a smaller band gap of $E_g = 0.009 \text{ eV}$ (red line in the figure). The decreased E_g value indicates a higher sensitivity of CFMS film to external influence, thus experimentally leading to the transition from semiconducting behavior to metallic behavior under the thermal disturbance at high measuring temperature as shown in Fig. 2(b).

In addition, we prepared a film of CFMS (10 nm) with Hall bar structure and measured the anomalous Hall effect (AHE) as shown in the inset of Fig. 2(a). The dependence of Hall resistivity ρ_{xy} on the applied field was shown in the inset of Fig. 2(a), in which the external field was along the perpendicular-to-film plane direction. According to the function [22]:

$$\rho_{xy} = R_0 H + R_s 4\pi M_{s\perp} \quad (1)$$

where R_0 and R_s are the ordinary and the anomalous Hall coefficient, respectively. We calculated the carrier concentration n_i dependence:

$$n_i = 1/eR_0 \quad (2)$$

The carrier concentration was found to be $5.3 \times 10^{20} \text{ cm}^{-3}$ at 300 K, which is closed to the previous report of CFMS system [16]. The negative value of R_0 also reveals the n -type semiconductor that is consistent with the previous work [12]. The electrical conductivity σ_{xx} of our sample is around $6.3 \times 10^3 \text{ S/cm}$, which is within the same magnitude with the reported value of $2.86 \times 10^3 \text{ S/cm}$ [16].

The bending tunability could be also reflected into the magnetic properties of the thin films. Fig. 3 shows the room temperature in-plane M - H curves of films under the flat and bending status, in which the CFMS film (20 nm) was fabricated and tested to confirm the bending tunable properties. Interestingly, an exchange bias was observed in both films without magnetic field annealing. The consistent results were obtained by choosing two bending curvatures. Under bending, the coercivity of both CFMS films was significantly enhanced, showing the increasing tendency of curvature, as shown in the insets of figure. At the smallest bending curvatures of 1.9 mm, the coercivities increase from 10 Oe to 54 Oe with an increment of the coercivity as high as 440% for the film with a thickness of 10 nm. The coercivity increases by 26 Oe in CFMS thin film with a thickness of 20 nm under the same bending curvature. The increase of coercivity may be explained by magnetocrystalline

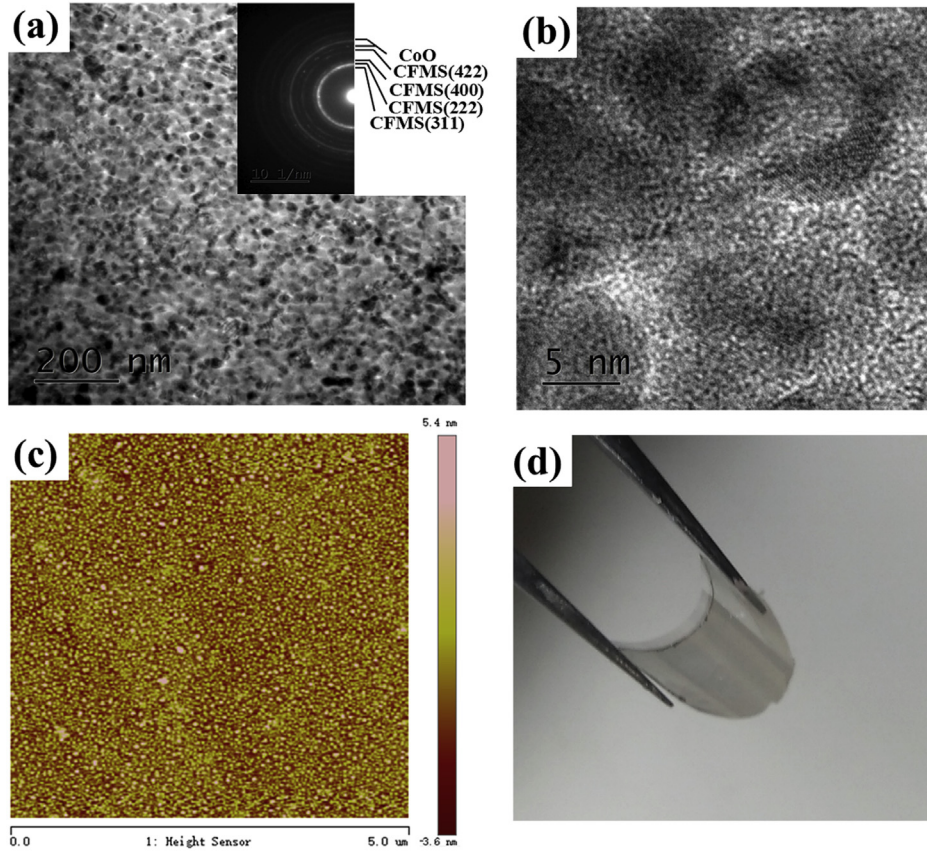


Fig. 1. Microstructure, surface morphology and bending flexibility of CFMS thin film (10 nm) annealed at 300 °C: (a) bright field TEM image with the inset of SAED pattern; (b) HRTEM image; (c) AFM image over $5 \times 5 \mu\text{m}$ area in 2-dimensional space; (d) bending image of flexibility.

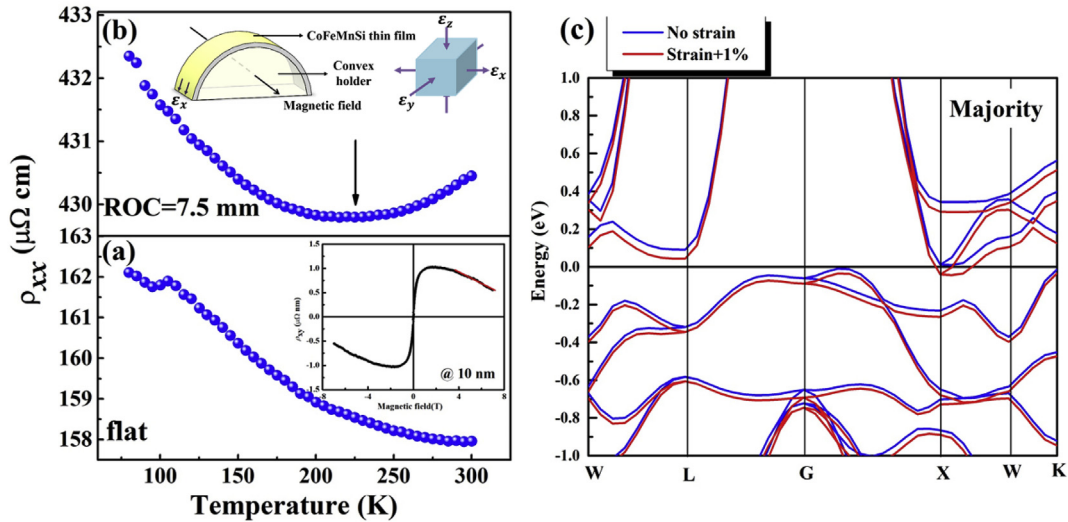


Fig. 2. Temperature dependence of the resistivity of the annealed CFMS (10 nm)/Pd film at 300 °C under (a) flat and (b) bending status; and the inset of Fig. 2(a) shows magnetic-field-dependent Hall resistivity ρ_{xy} at 300 K; the inset of Fig. 2(b) give the schematic of bending status; (c) majority-spin band structures of ordinary and bent CFMS.

anisotropy due to bending stress. However, the exchange bias does not show significant effects on the bending (the inset of figure), indicating the bending stability of exchange bias. On the other hand, we evaluated the saturation magnetization by the law of approach to saturation (LATs) method. The saturation magnetization decreased under the bending state in comparison to the flat

film for both films with the thicknesses of 10 nm and 20 nm.

The strain of the bending CFMS thin films can be evaluated by:

$$\varepsilon = (t_{\text{CFMS}} + t_{\text{F-mica}}) / 2R \quad (3)$$

where the t_{CFMS} and $t_{\text{F-mica}}$ are the thicknesses of the CFMS film and

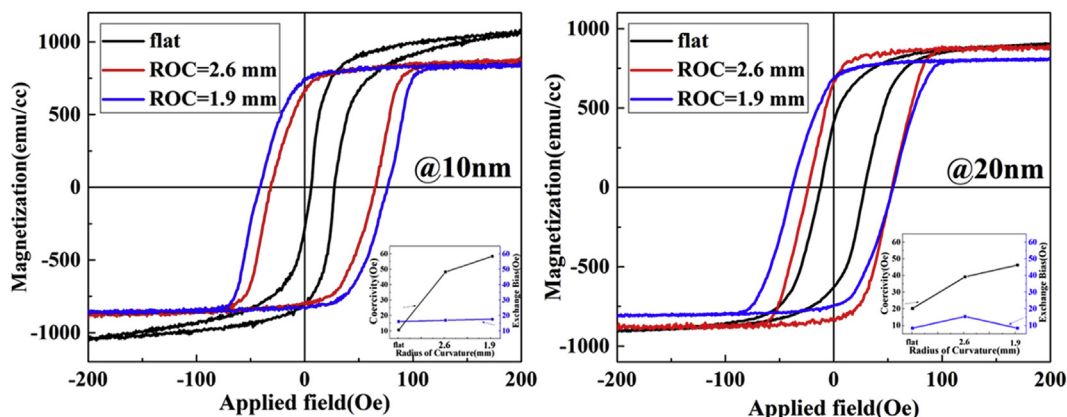


Fig. 3. Room temperature *M-H* loops of the annealed films under the flat and bending status with the thickness of (a) 10 nm, (b) 20 nm. The insets present the change of coercivity and exchange bias field under bending.

exfoliated F-mica substrate respectively. The *R* is the curvature of bending state. Owing to that the thickness of CFMS (10 nm) is much less than that (35 μm) of F-mica, we can ignore the contribution of CFMS thickness and the equation is simplified as:

$$\varepsilon = t_{F-mica}/2R \quad (4)$$

Taking into account that the thicknesses of F-mica and smallest curvature are 35 μm and 1.9 mm respectively, the biggest strain in this work is about 0.9%.

Fig. 3 shows that both films exhibit the feature of exchange bias, implying an antiferromagnetic coupling. As we know, the antiferromagnetic coupling is a common feature for the ferromagnetic metallic oxides. The coupling between antiferromagnetic and ferromagnetic layer which caused the phenomenon of exchange bias was found in 1956 by Bean and Meiklejohn [24,25], and there are some theory models explaining this phenomenon [25,26]. Besides, the ferromagnetic layer prepared on the organic substrate can also produces the exchange bias because of interfacial charge transfer [27,28]. In the current work, the fluorophlogopite substrate is a type of inorganic silicate oxides ($\text{KAl}_2(\text{AlSi}_3\text{O}_{10})(\text{OH})_2$). As analyzed by TEM, the weak interfacial reaction occurred between CoFeMnSi layer and substrate during sputtering and annealing

processes. Therefore, the exchange bias could originate from the interfacial antiferromagnetic coupling.

XPS analyses were performed to clarify the origin of exchange bias on the selected film CFMS (20 nm) annealed at 300 $^{\circ}\text{C}$. Fig. 4 gives the XPS spectra of Co 2p and Fe 2p along the film depth, in which the etching time represents the degree of depth. Regarding the XPS depth analyses, we first evaluated the time of etching whole CFMS film by varying the etching power. It should be noted that the case of etching 750 s indicates the region of interface between CFMS layer and F-mica substrate. According to the XPS handbook [29] and previous report [30], the peaks at 778.30 eV, 793.27 eV, 780.40 eV and 795.60 eV correspond to the metallic binding energies of Co 2p_{3/2} and Co 2p_{1/2}, the oxide binding energy of Co 2p_{3/2} and Co 2p_{1/2} of CoO respectively; and the peaks located at 707 eV, 720.1 eV, 710.9 eV and 724.5 eV correspond to the metallic binding energies of Fe 2p_{3/2} and Fe 2p_{1/2}, and Fe₂O₃ binding energy of Fe 2p_{3/2} and Fe 2p_{1/2}. It is very clear that the intensities of peaks corresponding to the oxide binding gradually increase with Ar ion etching. Thus, it can be deduced that there exists strong binding between ferromagnetic metallic atoms and O atoms, close to the oxides of CoO and Fe₂O₃ as shown in Fig. 4. The oxide of Fe₂O₃ possesses a high Neel temperature (~ 953 K) and the interfacial bonding of oxygen with the ferromagnetic metal could bring up the antiferromagnetic alignment of ferromagnetic atoms. That is, the antiferromagnetic coupling at the interface between CFMS and F-mica substrate will take place, causing the exchange bias [24–26].

4. Conclusions

In summary, we realized a flexible semiconductor-like CFMS thin film on the F-mica substrate through the mechanically exfoliation. It was found that there exists the bending tunability of the semiconductor-metal-like transition and coercivity. At the smallest bending curvature of 1.9 mm, the coercivities increase from 10 Oe to 54 Oe with an increment of the coercivity as high as 440% for the film with a thickness of 10 nm. The XPS analyses reveal that the exchange bias is originated from the antiferromagnetic coupling existing at the interface of CFMS and F-mica substrate.

Conflicts of interest

There are no conflicts to declare.

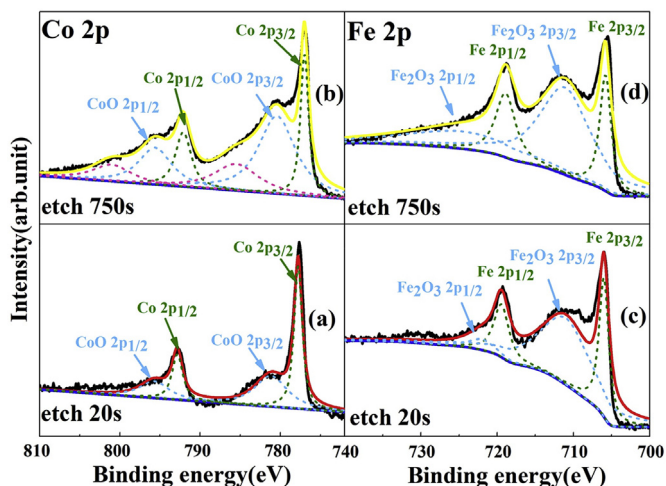


Fig. 4. XPS depth analyses of CFMS (20 nm) annealed at 300 $^{\circ}\text{C}$: (a)–(b) Co 2p spectrum and (c)–(d) Fe 2p spectrum.

Acknowledgements

This work was in part supported by the National Natural Science Foundation of China (Nos. 51771145, 51371140), Shaanxi key R & D plan, international scientific and technological cooperation and exchange program (No. 2017KW-020), Shaanxi Natural Science Basic Research Plan (No. 2017JM5060).

References

- [1] S.M. Ke, C. Chen, N.Q. Fu, H. Zhou, M. Ye, P. Lin, W.X. Yuan, X.R. Zeng, L. Chen, H.T. Huang, Transparent indium tin oxide electrodes on muscovite mica for high-temperature processed flexible opto-electronic devices, *ACS Appl. Mater. Interfaces* 8 (2016) 28406.
- [2] L.K. Shen, L. Wu, Q. Sheng, C.R. Ma, Y. Zhang, L. Lu, J. Ma, J. Ma, J.H. Bian, Y.D. Yang, A.P. Chen, X.L. Lu, M. Liu, H. Wang, C.L. Jia, Epitaxial lift-off of centimeter-scaled spinel ferrite oxide thin films for flexible electronics, *Adv. Mater.* 29 (2017) 1702441.
- [3] J. Gao, W. Guo, H. Geng, X. Hou, Z.G. Shuai, L. Jiang, Layer-by-layer removal of insulating few-layer mica flakes for asymmetric ultra-thin nanopore fabrication, *Nano Res.* 5 (2011) 99.
- [4] M.I.B. Utama, F.J. Belarre, C. Magen, B. Peng, J. Arbiol, Q.H. Xiong, Incommensurate van der Waals epitaxy of nanowire arrays: a case study with ZnO on muscovite mica substrates, *Nano Lett.* 12 (2012) 2146.
- [5] P.C. Wu, P.F. Chen, T.H. Do, Y.H. Hsieh, C.H. Ma, H.T. Duy, K.H. Wu, Y.J. Wang, H.B. Li, Y.C. Chen, J.Y. Juang, P. Yu, L.M. Eng, C.F. Chang, P.W. Chiu, L.H. Tjeng, Y.H. Chu, Heteroepitaxy of Fe₃O₄/muscovite: a new perspective for flexible spintronics, *ACS Appl. Mater. Interfaces* 8 (2016) 33794.
- [6] L.K. Shen, M. Liu, C.R. Ma, L. Lu, H.R. Fu, C.Y. You, X.L. Lu, C.L. Jia, Enhanced bending tuned magnetic properties in epitaxial cobalt ferrite nanopillar arrays on flexible substrate, *Mater. Horiz.* 5 (2018) 230.
- [7] Y. Zhang, L.K. Shen, M. Liu, X. Li, X.L. Lu, L. Lu, C.R. Ma, C.Y. You, A.P. Chen, C.W. Huang, L. Chen, M. Alexe, C.L. Jia, Flexible quasi-two-dimensional CoFe₂O₄ epitaxial thin films for continuous strain tuning of magnetic properties, *ACS Nano* 11 (2017) 8002.
- [8] W.L. Liu, M. Liu, R. Ma, R.Y. Zhang, W.Q. Zhang, D.P. Yu, Q. Wang, J.N. Wang, H. Wang, Mechanical strain-tunable microwave magnetism in flexible CuFe₂O₄ epitaxial thin film for wearable sensors, *Adv. Funct. Mater.* 28 (2018) 1705928.
- [9] Q. Yang, Z.Y. Zhou, L.Q. Wang, H.J. Zhang, Y.X. Cheng, Z.Q. Hu, B. Peng, M. Liu, Ionic gel modulation of RKKY interactions in synthetic anti-ferromagnetic nanostructures for low power wearable spintronic devices, *Adv. Mater.* 30 (2018) 1800449.
- [10] L.K. Shen, G.H. Lan, L. Lu, C.R. Ma, C.M. Cao, C.J. Jiang, H.R. Fu, C.Y. You, X.L. Lu, Y.D. Yang, L. Chen, M. Liu, C.L. Jia, A strategy to modulate the bending coupled microwave magnetism in nanoscale epitaxial lithium ferrite for flexible spintronic devices, *Adv. Sci.* 5 (2018) 1800855.
- [11] X.L. Wang, Proposal for a new class of materials: spin gapless semiconductors, *Phys. Rev. Lett.* 100 (2008) 156404.
- [12] H.R. Fu, C.Y. You, F.Q. Xin, L. Ma, N. Tian, Electric-field tuning of magnetism in spin gapless semiconductor (SGS)-like CoFeMnSi thin film, *Appl. Phys. Lett.* 112 (2018) 262406.
- [13] L. Bainsla, A.I. Mallick, M.M. Raja, A.K. Nigam, B.S.D.C.S. Varaprasad, Y.K. Takahashi, A. Alam, K.G. Suresh, K. Hono, Spin gapless semiconducting behavior in equiatomic quaternary CoFeMnSi Heusler alloy, *Phys. Rev. B* 91 (2015) 104408.
- [14] G.Z. Xu, E.K. Liu, Y. Du, G.J. Li, G.D. Liu, W.H. Wang, G.H. Wu, A new spin gapless semiconductors family: quaternary Heusler compounds, *Europhys. Lett.* 102 (2013) 17007.
- [15] J.C. Han, Y.L. Feng, K.L. Yao, G.Y. Gao, Spin transport properties based on spin gapless semiconductor CoFeMnSi, *Appl. Phys. Lett.* 111 (2017) 132402.
- [16] V.K. Kushwaha, J. Rani, A. Tulapurkar, C.V. Tomy, Possible spin gapless semiconductor type behaviour in CoFeMnSi epitaxial thin films, *Appl. Phys. Lett.* 111 (2017) 152407.
- [17] X.T. Wang, Z.X. Cheng, J.L. Wang, X.L. Wang, G.D. Liu, Recent advances in the Heusler based spin-gapless semiconductors, *J. Mater. Chem. C* 30 (2016) 7176–7192.
- [18] Y. Jin, P. Kharel, S.R. Valloppilly, X.Z. Li, D.R. Kim, G.J. Zhao, T.Y. Chen, R. Choudhary, A. Kashyap, R. Skomski, D.J. Sellmyer, Half-metallicity in highly L₂₁-ordered CoFeCrAl thin films, *Appl. Phys. Lett.* 109 (2016) 142410.
- [19] P. Kharel, W. Zhang, R. Skomski, S. Valloppilly, Y. Huh, R. Fuglsby, S. Gilbert, D.J. Sellmyer, Magnetism, electron transport and effect of disorder in CoFeCrAl, *J. Phys. D Appl. Phys.* 48 (2015) 245002.
- [20] Y. Jin, R. Skomski, P. Kharel, S.R. Valloppilly, D.J. Sellmyer, Effect of disorder on the resistivity of CoFeCrAl films, *AIP Adv.* 7 (2017), 055834.
- [21] Y. Feng, H. Chen, H.K. Yuan, Y. Zhou, X.R. Chen, The effect of disorder on electronic and magnetic properties of quaternary Heusler alloy CoFeMnSi with LiMgPbSb-type structure, *J. Magn. Magn. Mater.* 378 (2015) 7.
- [22] L. Bainsla, R. Yilgin, M. Tsujikawa, K.Z. Suzuki, M. Shirai, S. Mizukami, Low magnetic damping for equiatomic CoFeMnSi Heusler alloy, *J. Phys. D Appl. Phys.* 51 (2018) 495001.
- [23] Q. Zhang, H.R. Fu, C.Y. You, L. Ma, N. Tian, Perpendicular magnetic anisotropy and hydrogenation-induced magnetic change of Ta/Pd/CoFeMnSi/MgO/Pd multilayers, *Nanoscale Res. Lett.* 13 (2018) 222.
- [24] W.H. Meiklejohn, C.P. Bean, New magnetic anisotropy, *Phys. Rev.* 102 (1956) 1413–1414.
- [25] W.H. Meiklejohn, C.P. Bean, New magnetic anisotropy, *Phys. Rev.* 105 (1957) 904–913.
- [26] D. Mauri, H.C. Siegmann, P.S. Bagus, E. Kay, Simple model for thin ferromagnetic films exchange coupled to an antiferromagnetic substrate, *J. Appl. Phys.* 62 (1987) 3047–3049.
- [27] Q. Zhang, W.B. Mi, X.C. Wang, Antiferromagnetic order at the first Fe₄N atomic layer in benzene adsorbed Fe₄N structures, *J. Phys. Chem. C* 119 (2015) 23619–23626.
- [28] M.F. Sun, X.C. Wang, W.B. Mi, Spin polarization and magnetic characteristics at C₆H₆/Co₂MnSi(001) spinterface, *J. Chem. Phys.* 147 (2017) 114702.
- [29] J.F. Moulder, W.F. Stickle, P.E. Sobol, K.D. Bomben, Handbook of X-Ray Photoelectron Spectroscopy: a Reference Book of Standard Spectra for Identification and Interpretation of XPS Data, Perkin-Elmer, Boca Raton, FL, 1992.
- [30] N.Y. Sun, Y.Q. Zhang, H.R. Fu, W.R. Che, C.Y. You, R. Shan, Perpendicular magnetic anisotropy in Mn₂CoAl thin film, *AIP Adv.* 6 (2016), 015006.